17th World Conference on Earthquake Engineering, 17WCEE

Sendai, Japan - September 13th to 18th 2020

NUMERICAL STUDY ON THE SEISMIC PERFORMANCE OF POSTTENSIONED CFST HYBRID BRIDGE COLUMNS

Y. Shen[(1)], J. Li[(2)], Y. Li[(3)], W. Guo[(4)]

[(1)] *Ph.D. Candidate, School of Civil Engineering, Tongji University, Shanghai, China, yushen@tongji.edu.cn*
[(2)] *Professor, School of Civil Engineering, Tongji University, Shanghai, China, lijianzh@tongji.edu.cn*
[(3)] *Ph.D. Candidate, School of Civil Engineering, Tongji University, Shanghai, China, yongxing_lee@tongji.edu.cn*
[(4)] *Ph.D., T.Y.Lin International Engineering Consulting (China) Co., Ltd., Chongqing, China, guowei@tylin.com.cn*

Abstract

Conventional reinforced concrete bridge columns, under the prevailing ductility capacity design concepts, are anticipated to exhibit inelastic behavior within the localized flexural plastic hinge regions. However, this philosophy may lead to permanent residual drift and serve concrete damage in the bridge columns during the design-level earthquakes. An attractive technology combines a precast posttensioned concrete filled steel tubular (CFST) column, with embedded mild reinforcement, in a way to resist the same seismic actions while experiencing limited damage and residual offsets. In this hybrid system, unbonded post-tensioned (PT) tendons are passed through the column to provide recentering ability. The steel tube not only serves as a formwork for casting, but also provides the enhanced confinement effects. Mild reinforced bars, also referred to as energy dissipation (ED) bars, are only used at the column ends to enhance the seismic resistance of the column.

The objectives of this study were to numerically explore (1) the influence of different key parameters on the cyclic response of CFST hybrid columns and (2) the seismic behavior of a conventional bridge incorporating this column. First, a nonlinear finite element (FE) model of this hybrid single-column pier was developed using the OpenSees software package. Based on the established analysis model of the column, a series of quasi-static cyclic analyses were carried out to systematically investigate the effects of diameter-to-thickness (D/t) ratio, slenderness ratio, post-tensioning force, and amount of longitudinal mild reinforcement on hysteretic responses. Furthermore, nonlinear time-history analyses of a typical four-span highway bridge with the posttensioned CFST hybrid columns were conducted. The analysis results confirmed the potential benefits of a combination of the unbonded PT tendons, steel tube and mild steels in bridge columns under seismic loadings. The study results also indicated that the internal mild steels can provide ED capacity by axial yielding at the expense of the increasement of residual drift. In addition, the slenderness ratio and the amount of ED bars had a pronounced impact on the lateral load capacity of the CFST hybrid columns.

Keywords: bridge columns; seismic; concrete filled steel tube; post-tensioning; numerical simulation

1. Introduction

Under the ductility design concept, conventional reinforced concrete bridge columns are expected to exhibit inelastic behavior within the plastic hinge regions. However, this philosophy may lead to significant residual displacement and serve damage for concrete and steel reinforcement bars in the bridge columns under the strong earthquakes. As a result, traffic closure for assessment, repair or demolition of the damaged columns is inevitable, and the corresponding economic losses are huge. In order to reduce or eliminate these impacts on post-earthquake traffic, more and more attention has been paid on the self-centering systems, which can survive strong earthquakes with less damage [1-4]. The concept of controlled rocking in bridge columns is a typical self-centering behavior, which can be achieved by using a combination of unbonded post-tensioning (PT) and local hysteretic energy dissipation (ED) devices. In this hybrid column system, the capacity of self-centering is provided by the post-tensioning and gravity loads, and the former is the main contributor. Energy dissipation occurs through yielding of the internal or external energy dissipators, which located across the column-footing and column-cap interfaces. With a designed combination of the PT force and the ED devices, as seen in Fig.1, an idealized flag-shaped hysteretic response that owns both the acceptable residual displacement and adequate energy dissipation can be obtained.

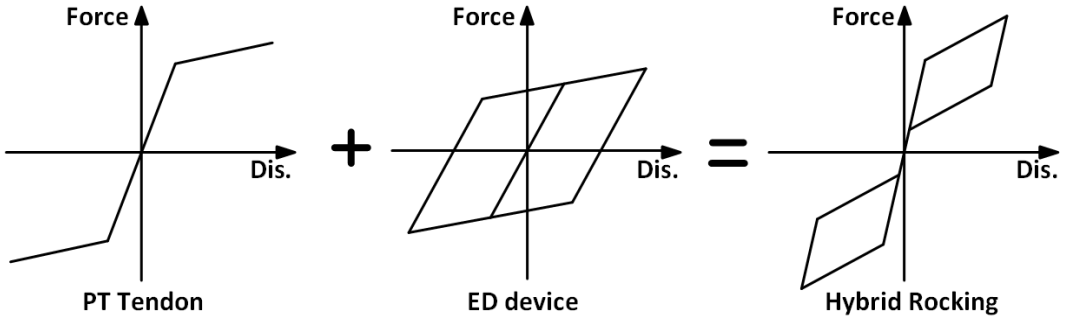

Fig. 1 – Composition of the idealized Flag-shaped hysteretic curve

The early development of the hybrid system was mainly focused on implementation in buildings; and the interest in the use of rocking systems in bridges increased in the last two decades [3]. From a numerical investigation on the monotonic, cyclic and seismic behavior of unbonded PT concrete bridge piers with internal mild steel, Kwan et al. [5,6] found that that there was a trade-off between the energy dissipation and the residual displacement. The tailoring of optimal designs of this column could be realized by varying the ratio of unbonded posttensioning to internal mild reinforcement. Marriott et al. [7, 8] expanded this idea and adopted external energy dissipators into the experimental studies of hybrid rocking piers. The test results showed that this type pier outperforms a traditional conventional ductile pier in terms of inherent stability, extent of damage and self-centering capacity. Similar investigation of the effect of yielding level and post-yielding stiffness ratio of ED bars on the seismic response of PT rocking bridge piers has been conducted by Roh et al. [9]. It was found that the influence of these two parameters become small when the ED bars have a higher yielding moment. In addition, the seismic response of precast segmental column with PT tendons and ED bars across the segment-to-segment interfaces has also been investigated by Wang et al. [10].

To avoid the earlier crushing of concrete at the interfaces owing to high compressive stresses, the outer steel tube is used to encase the concrete. This composite member is called concrete-filled steel tube (CFT) column. The tube replaces the formwork during construction, acts as transverse reinforcement and provides significant confining pressure to the concrete. Based on these advantages, the seismic behavior of post-tensioned CFT segmental bridge columns in which bottom segment encased by steel tube was experimentally and numerically investigated by some researchers [11-14]. Hayashi et al. [15] indicated that a self-centering rocking frame system where double-skin HS CFT columns were adopted could show satisfactory seismic performance. From a comparison test of the self-centering CFST columns with different arrangements of the PT strands and energy dissipaters, Wang et al. [16] found that all specimens exhibited

flag-shaped hysteretic behavior with an expected deformation mode and good self-centering capacity. Apart from the steel tube, the FRP is alternative material that can be used to confine the concrete [17].

In this paper, the cyclic responses of the CFST hybrid rocking columns and the seismic behavior of a conventional bridge incorporating this column were numerically investigated. First, based on the OpenSees software package, a detailed finite element (FE) model of a typical CFST hybrid column with internal ED bars is developed. Then, parametric analyses are conducted to investigate the effect of different parameters on the cyclic. The concerned parameters include the diameter-to-thickness (D/t) ratio, the slenderness ratio, the PT force, and the amount of ED bars. Finally, a dynamic analysis is carried out to explore and quantify the differences between CFST bridges with and without initial PT force.

2. Bridge Column and Finite Element Model

2.1 Bridge column information

To investigate the effect of key parameters on the cyclic response, a typical posttensioned CFST hybrid rocking bridge column was adopted for the numerical simulation in this study. As shown in Fig. 2(a), the superstructure of the bridge was comprised of decks and eight type-I girders. Each bridge bent cap, with a height of 1.6 m, was supported by a circular posttensioned CFST column. A dead weight, *G*, supported by the single column was take as 4.57 MN (equal to 5% axial load ratio). The clearance height of the column (*H*) was 9.0 m, and the diameter (*D*) was 1.5 m, resulting in a slenderness ratio of 6.0. The thickness of steel tube (*t*) was 16 mm. Consequently, the diameter-to-thickness and the ratio of steel tube were 94 and 4.22%, respectively. The column had 32 #28 longitudinal steel bars at both column ends, providing a longitudinal reinforcement ratio, ρ_{ED} of 1.18%. A total 15.24 cm diameter strand was employed to be the unbonded PT tendon, which was placed at the center of the cross section and debonded along the full height of the column. The initial PT force, *P*, applied into the tendon was also designed to be 4.57 MN or 5% axial load ratio, resulting in a total axial load ratio of 10%. The total unbonded length of the PT tendon was 10.5 m.

To prevent undesirable premature fracture of ED bars, the minimum unbonded length of the energy dissipaters L_u can be calculated by [18]

$$L_u \geq \varepsilon_{cu} / \varepsilon_{su} \times (d_s - c) + L_{sp} \tag{1}$$

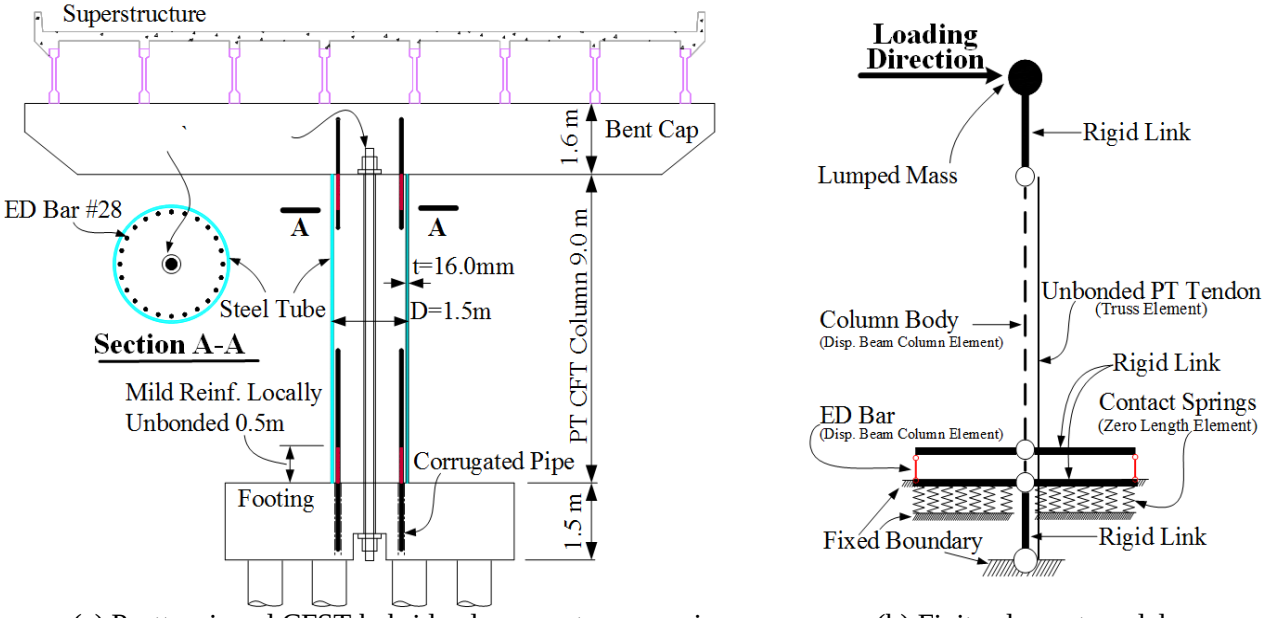

(a) Posttensioned CFST hybrid column system overview (b) Finite element model

Fig. 2 – Schematic diagram of the hybrid CFST rocking column and the finite element model

where ε_{cu} and ε_{su} are the ultimate compressive strain of confined concrete and ultimate tensile strain of the ED bars, respectively; d_s is the diameter of circle encompassing energy bars; c is the neutral axis depth at joint, which is recommended not to exceed 20% of the column diameter at the target lateral drift [19]; L_{sp} is the length of strain penetration, and can be taken as [20]:

$$L_{sp} = 0.15 f_y d_b \tag{2}$$

where f_y and d_b are the tensile yield strength and the diameter of ED bars. In this study, according to the Eqs. (1) and (2), the unbonded length of the ED bars was selected to be 0.5m.

2.2 Finite element model

A FE model of the bridge column, which is shown in Fig. 2(b), was built to perform the cyclic analysis. In that model, three displacement beam-column fiber elements in series were adopted to model the behavior of the column. The masses of the cap beam and the superstructure were concentrated in the top loading point. Regions from the column bottom to the base (bottom anchorage point of PT tendon) and the column top to the loading point were linked with rigid bars. The Concrete01 material model was used for the concrete of the column body, with uniaxial stress–strain relationship developed by Han et. al [21]. The stress–strain model for circular section is shown as following:

$$y = 2x - x^2 \quad (x \le 1) \tag{3}$$

$$y = \begin{cases} 1 + q(x^{0.1\xi} - 1) & (\xi \ge 1.12) \\ \dfrac{x}{\beta(x-1)^2 + x} & (\xi < 1.12) \end{cases} \quad (x > 1) \tag{4}$$

where $x=\varepsilon/\varepsilon_0$, $y=\sigma/\sigma_0$ with ε_0 and σ_0 representing the peak stress and the corresponding strain, respectively; β is related to the shape and material properties of the steel tube; ξ is the confinement factor, which can be expression by:

$$\xi = \frac{A_s f_y}{A_c f_{ck}} \tag{5}$$

where A_s and A_c are the section areas of the steel tube and encased concrete, respectively; f_s is the yield strength of the steel tube, f_{ck} is the characteristic strength of the concrete. The more detailed information on the stress–strain relationship of concrete can be found in the monograph [21]. In this study, the ξ is calculated to be 0.567, and the ε_0 and σ_0 are calculated to be as 0.00323 and 38.99 MPa, respectively.

The Steel02 material model, based on the uniaxial Giuffre-Menegotto-Pinto model, was assigned to the axial and flexural relationship of the ED bars, and the torsional response was considered elastic. The yield strength, elastic modulus and strain-hardening ratio was assumed to be 335 Mpa, 200 Gpa and 0.01, respectively. The parameters to control the the transition from elastic to plastic branches R_0, c_{R1} and c_{R2} were seletced as 18, 0.925 and 0.15, respectively, while no isotropic harding was considered. As shown in Fig. 2(b), the lower ends of the ED bars were fixed to the ground, while the upper ends were connected to the column body with radial rigid arms. Becasue the PT tendons should remain to be elatic before achieving the target lateral drift, the elastic truss element with a modulus of elasticity of 195 Gpa was adopted to model the behavior.

A series of zero-length elements were adopted to represent the contact and opening at the interface between the column and footing. The interface was discretized into 36 wedges along the circumference, and 10 rings along the radius, resulting in a total of 360 elements. Considering that only compressive strength needed to be included into the contact springs and neglected the tensile behavior, the Elastic-No Tensile material was utilized for the contact simulation. According to the findings of Yamashita et. al [2], the contact stiffness can be calculated by dividing the elastic modulus of the concrete by the effective thickness of the contact element h_e, which can be expressed by:

$$h_e = \begin{cases} t_1 h_0 \left(\frac{t_1 + t_2}{2t_1 t_2} - \frac{1}{t_2}\right) & \text{for} \quad h \geq h_0 \\ t_1 h \left(\frac{t_1 + t_0}{2t_1 t_0} - \frac{1}{t_2}\right) & \text{for} \quad h \leq h_0 \end{cases} \tag{6}$$

where h is the thickness of the footing; t_1 and t_2 are, respectively, the dimensions of the column and the footing in the perpendicular direction to the loading direcion; h_0 and t_0 are also the parameters related to the dimensions of the column and footing. In this study, the contact stiffness was calculated to be 50.73 N/mm^3.

3. Parametric analysis

Based on the established FE model of the posttensioned CFST hybrid column, a parametric analysis covering the influences of PT force ratio (P/f_cA_g), slenderness ratio (H/D), diameter-to-thickness (D/t) and ratio of ED bars, ρ_{ED}, was conducted. The detailed values of these four parameters are listed in Table 1. As shown in Table 1, each parameter has four variable values, which resulted in a total of 13 quasi-static analytical cases. The displacement-control schedule with 12 drift levels was adopted. A single cycle was applied at drift ratios of 0.1%, 0.3%, 0.5%, 1.0%, 1.5%, 2.0%, 2.5%, 3.0%, 3.5%, 4.0%, 4.5% and 5.0%. The drift ratio is the ratio of the column lateral displacement to the column clearance height.

Table 1 – Variables of parametric analysis

Variables	Values
PT force ratio, P/f_cA_g	0% (P=0 MN), 5% (P=4.57 MN),10% (P=9.14 MN) and 15% (P=13.71 MN)
Slenderness ratio, H/D	4 (H=6.0 m), 6 (H=9.0 m), 8 (H=12.0 m) and 10 (H=15.0 m)
Diameter-to-thickness, D/t	94 (t=16 mm), 150 (t=10 mm), 375 (t=4 mm) and ∞ (t=0 mm)
ED bars ratio, ρ_{ED}	0% , 0.57% (32 #20), 1.12% (32 #28) and 1.84% (32 #36)

3.1 Influence of PT force

Fig. 3 shows the effect of changing the initial PT force on the cyclic responses of the posttensioned CFST column. The applied initial PT forces ranged from 0% to 15% with an interval of 5%, resulting in four cases of a total axial load ratio of 5%, 10%, 15% and 20%. From the Fig. 3(a), which shows the hysteretic and backbone curves of these four initial PT forces, it can be found that the applied initial PT force had a positive effect on the load capacity of the posttensioned CFST columns. The load capacity of the column with 15% initial PT force ratio was about 1.6 times larger than that of the column without inital PT force at the 5% lateral drift ratio.

Fig. 3(b) shows the stiffness ratio K_i/K_e verses the lateral drift relationship, in which K_e is the initial stiffness and K_i is the secant stiffness of ith cycle number. It can be seen that with the increase of inital PT force, the magnitude of the initial stiffness increased, especailly in ther range [0%, 5%] with a increase from 14.78 MN/m to 23.65 MN/m. However, the influence of the initial PT force on the stiffness ratio K_i/K_e was not siginificant, and four curves of K_i/K_e have the similar decay trend. All columns had a fast stiffness degradation before the drift ratio of 1%, and after that, a relatively mild decay of stiffness can be observed. Exceeding 3% drift ratio, the secant stiffness remained almost constant.This phenomenon is similar to the test results of Qian et al. [22].

As to the influence of initial PT force on the residual drift of the posttensioned CFST column, which was shown in Fig. 3(c), the increse of the intial PT force resulted in a tremendous reduction in the residual displacement. In this analyzed column, when the initial PT force equal to 10%f_cA_g, the residual deformation can nearly be eliminated. In addition, it can also be seen that although the applied lateral force was removed, the residual drift led to the increase of the initial PT force (ΔPT).

The energy dissipation, E, and the equivalent viscous damping, ξ, at each drift ratio were shown in Fig. 3(d). The energy dissipation was calculated by using the area of each hysteretic loop and the equivalent viscous damping was calculated by using Eq. (7):

$$\xi = \frac{E}{4\pi \times E_{strain}} \tag{7}$$

where E_{strain} is the strain energy measured at the peak force. For the same lateral drift ratio, the differences of energy dissipation between four initial PT forces were small; however, the column with PT=0% had the highest value of the equivalent viscous damping because of its the highest peak force. This phenomenon indicated that the enhanced self-centering capacity owing to the increase of initial PT force will weaken the capacity of energy dissipation. In addition, the increasing equivalent viscous damping became almost stable when the stiffness ratio K_i/K_e reached the relatively fast degradation phase.

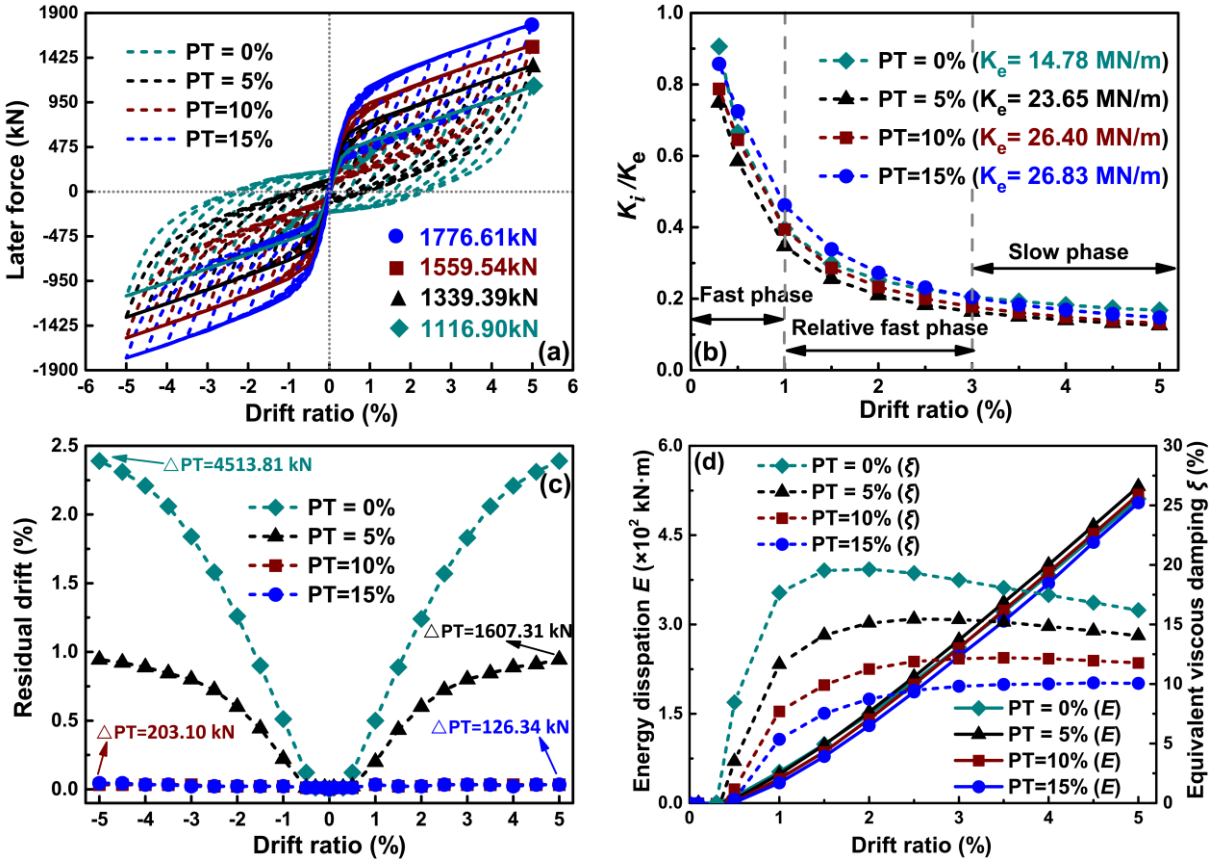

Fig. 3 responses with different initial PT forces: (a) hysteretic and backbone curves; (b) stiffness degradation; (c) residual drift and (d) energy dissipation and equivalent viscous damping

3.2 Influence of slenderness ratio

Similarly, the influence of changing the slenderness ratio on the cyclic responses of the posttensioned CFST column is shown in Fig. 4. The columns had four different slenderness ratios of 4, 6, 8 and 10, which were related to column height of 6.0 m, 9.0 m, 12.0 m and 15.0 m, respectively. Based on the observation of the hysteretic responses in Fig. 4(a), it can be concluded that the load capacity of the posttensioned CFST column will decrease dramatically with the increase of the column height. There were two primary reasons for the above phenomenon. One was the P-Δ effect when the column rocked, which led to a more severe extra displacement in the column with high slenderness ratio. The other was the effect of the length of PT tendon. For the same drift ratio, the increasing PT force in the column with a higher height, which was advantageous to the load capacity, was relatively smaller. Apart from the load capacity, the initial stiffness of

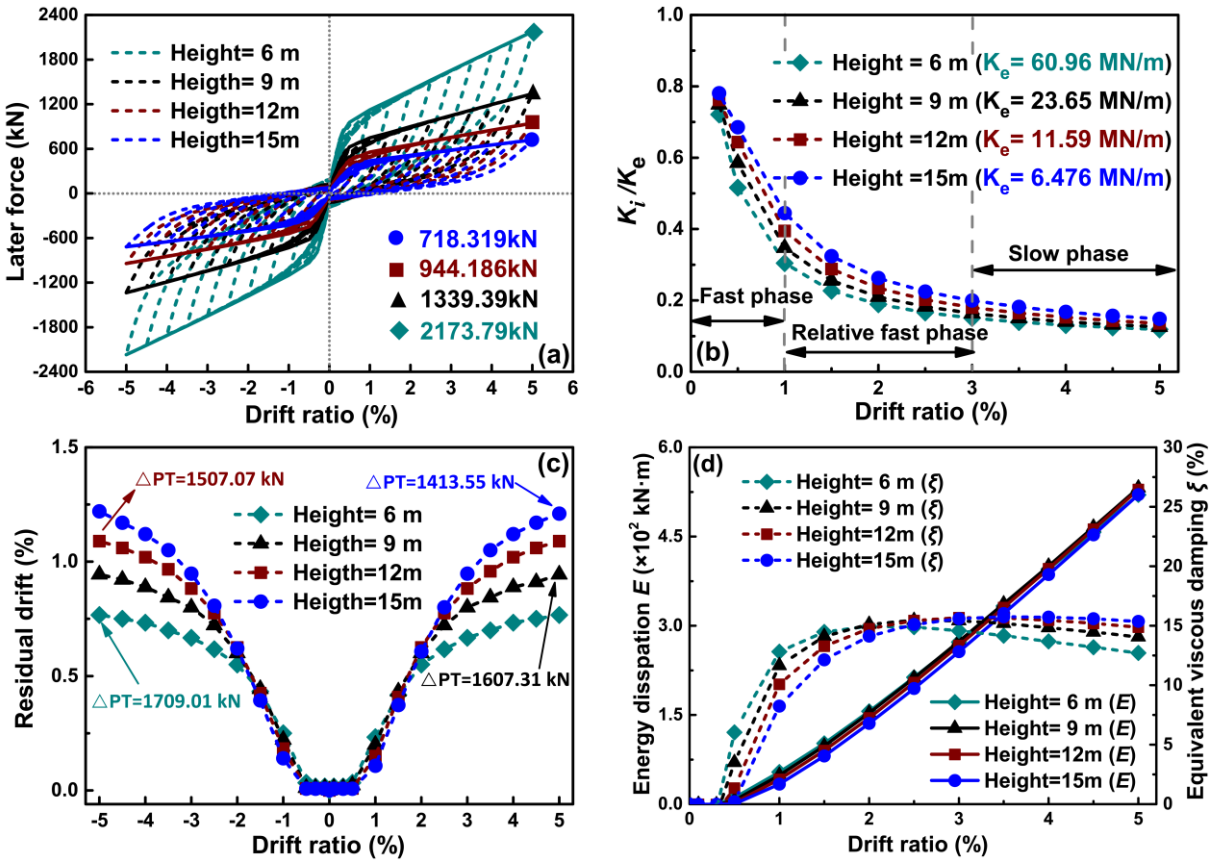

Fig. 4 responses with different slenderness ratios: (a) hysteretic and backbone curves; (b) stiffness degradation; (c) residual drift and (d) energy dissipation and equivalent viscous damping

the column also showed a serious decline because of the increase of slenderness ratio, as illustrated in Fig. 4(b). In addition, all columns likewise experienced three stiffness degradation phases: fast degradation phase (0%-1% drift ratio), relatively fast degradation phase (1%-3% drift) and slow degradation phase (3%-5% drift), without obvious differences.

From the Fig. 4(c), which shows the influence of the slenderness ratio on the residual drift, it can be seen that when the applied lateral drift ratio was less than 0.5%, all columns can restore to their original positons because of the posttensioning force of tendon. However, with the further increase of the applied lateral drift ratio, the residual deformation occurred and continuously increased. It should be noted that although the higher slenderness ratio can lead to the increase of the residual drift, the increment of the initial PT force (ΔPT) decreased, which was caused by the length of PT tendon. Fig. 4(d) shows the energy dissipation and the equivalent viscous damping curves for all columns with four different slenderness ratios. By comparison the results, it can be found that there was a slight difference in the dissipated energy between columns with different slenderness ratios

3.3 Influence of diameter-to-thickness

The diameter-to-thickness is an important parameter when designing CFST column, and its influence on the cyclic responses is shown in Fig. 5. The selected tube thicknesses were 0 mm, 4 mm, 10 mm and 16 mm, and the corresponding diameter-to-thickness were 94, 150, 375 and ∞. It should be noted that the case with t= 0 mm is the posttensioned reinforced concrete (RC) column, whose stress–strain relationship of the confined concrete should adopt the equations developed by Mander et. al [23].

Fig. 5(a) compares the hysteretic and backbone curves of the bridge PT column with different steel tube thicknesses. It can be observed that the use of the steel tube can enhance the load capacity because of

the differences of the stress–strain curve. At the drift ratio of 5%, the lateral force of the recentering CFST column with t=4 mm was 21.4% greater than that of the recentering RC column. In addition, the increase of tube thickness also amplified the initial stiffness of the column, as shown in Fig. 5(b). The recentering RC column showed the faster stiffness degradation than the recentering CFST column due to the weaker restraint effect of the stirrups.

It should be mentioned that the load capacity and stiffness of the recentering RC column were lower than those of the recentering CFST column; However, the residual drift of these two kind columns, shown in Fig. 5(c), were almost the same, except for the CFST column with tube of 4 mm. The probable reason for this phenomenon is that the concrete of the rocking toe was crushed in the RC column, which resulted in the increase of the neutral axis depth and the decrease of rocking height of the interface. This interpretation can be proven by the fact that at the drift ratio of 5%, the joint opening values for recentering RC column and recentering CFST column with t=16 mm were 33.56 mm and 51.78 mm, respectively. As to the energy dissipation of columns with different D/t in Fig. 5(d), the recentering CFST with t=16 mm showed the best capacity of energy dissipation; however, the RC column showed the highest equivalent viscous damping.

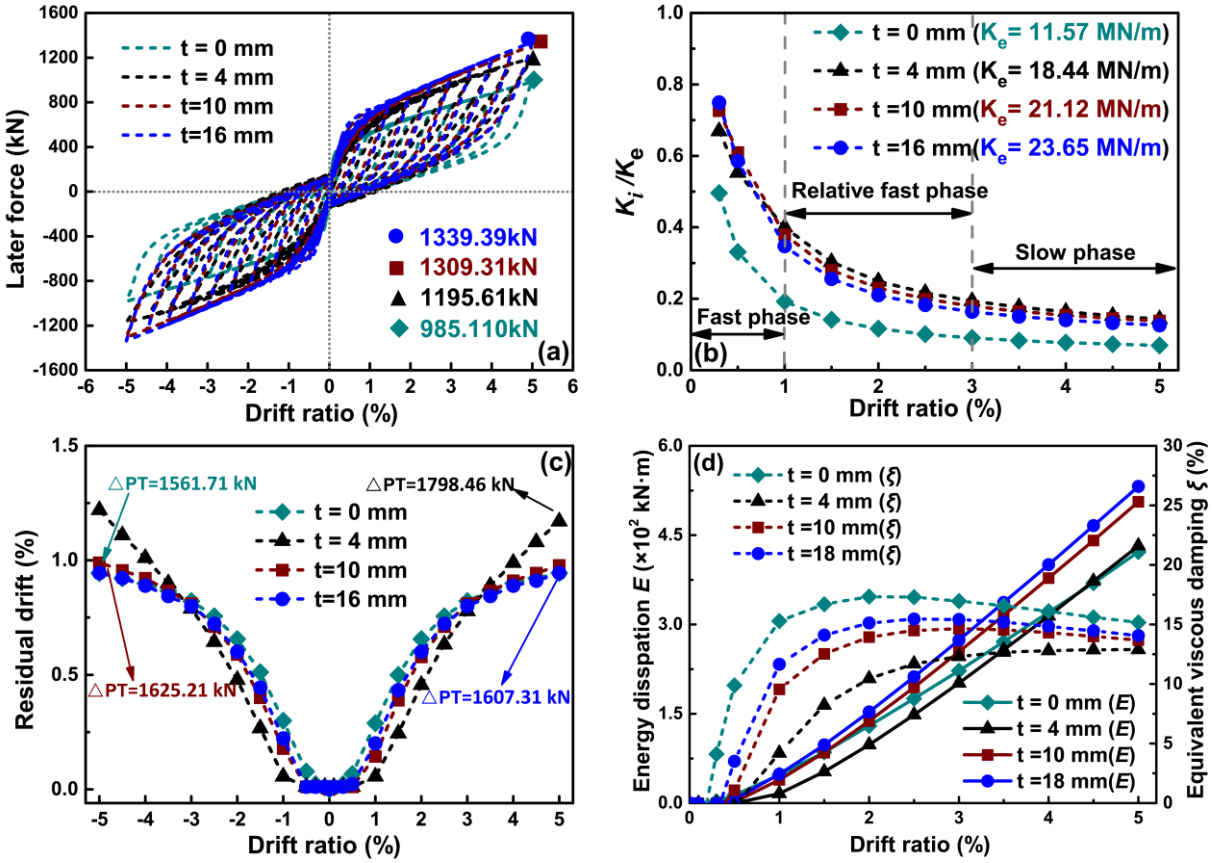

Fig. 5 responses with different D/t ratios: (a) hysteretic and backbone curves; (b) stiffness degradation; (c) residual drift and (d) energy dissipation and equivalent viscous damping

3.4 Influence of amount of the ED bars

Fig. 6(a) shows the lateral strength versus drift ratio of the posttensioned CFST columns with four different diameters of the ED bars, i.e., diameter of 0 mm, 20mm, 28mm and 36mm. From the figure, a pure rocking hysteretic curve can be observed for the column without ED bars, which was similar to the left force-displacement relationship of Fig. 1. This indicated that in this column, the drifts were mainly caused by rotations as a rigid body around the toes of the column, and deformation of the column body was minimal or even negligible. In addition, the increase of the amount of ED bars was beneficial to the load capacity and

the initial stiffness of the posttensioned CFST columns. The increasing amount of the ED bars can also decrease the trend of stiffness degradation, as shown in Fig. 6(b).

By comparing between Figs. 6(c) and (d), the capacity of energy dissipation of posttensioned CFST columns, as expected, can be enhanced when the amount of ED bars increased; However, the residual drift also rapidly increased. This means that the energy-dissipation capacity and the recentering capacity are contradictory. Thus, attentions needs to be paid to obtaining satisfactory hysteretic performance, which is characterized by acceptable residual displacement and adequate energy dissipation.

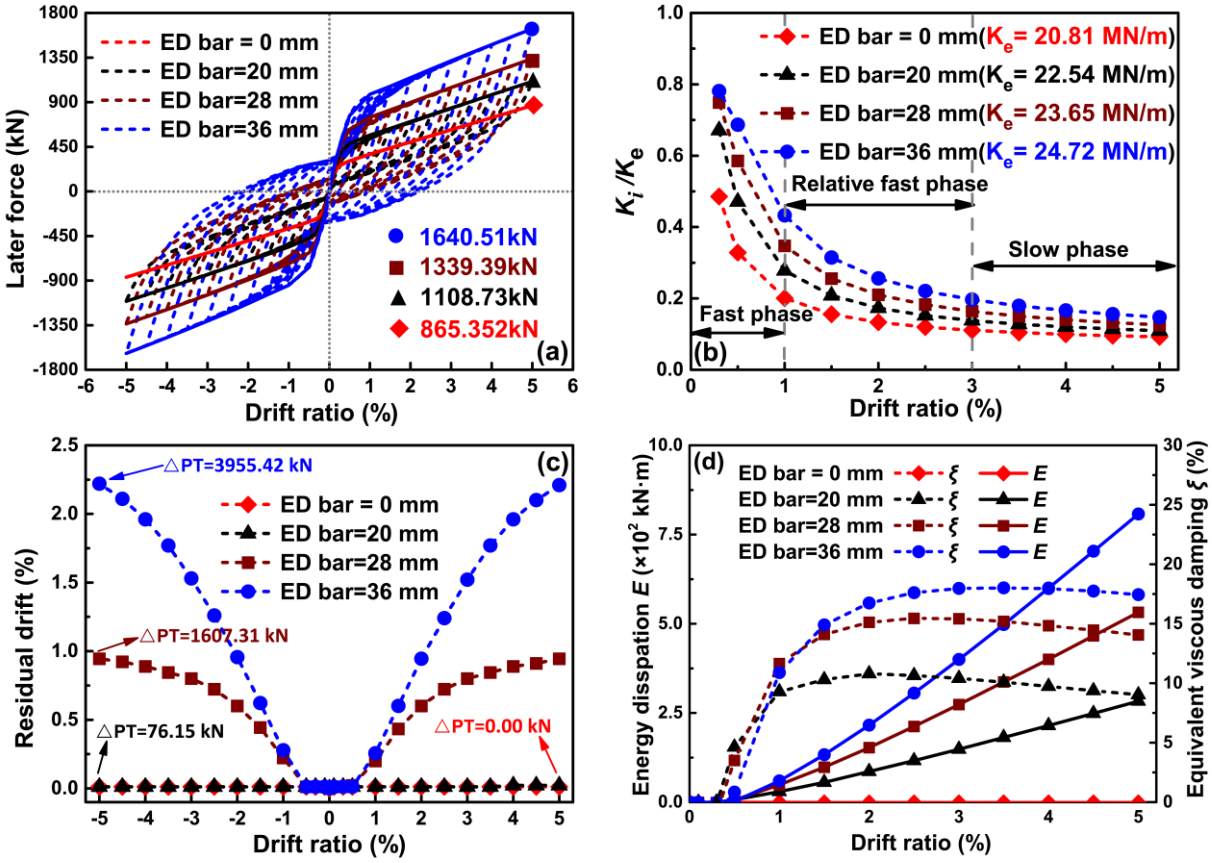

Fig. 6 responses with different amounts of ED bars: (a) hysteretic and backbone curves; (b) stiffness degradation; (c) residual drift and (d) energy dissipation and equivalent viscous damping

4. Dynamic response of bridges with posttensioned CFST columns

4.1 Prototype bridge background

To validate the effectiveness of employing posttensioned CFST columns in dynamic response of bridge, a typical continuous girder bridges was adopted for the numerical simulation. As shown in Fig.7, the four-span bridge had a total length of 120.0 m, with span arrangement of 4×30.0 m. The dimensions of columns described in subsection 2.1 were used in this bridge and the bearing arrangement are also shown in Fig.7. The friction behavior of sliding bearings can be modeled by a bilinear hysteretic model, in which the yield stiffness and the yield displacement were set as to 0 and 2 mm, respectively. It should be noted that the identical FE model of the structure with initial PT force of $5\%f_cA_g$ in columns was also used for the numerical simulation of the structure without including initial PT force, while the initial PT force was set as zero for the latter model. The damping ratio of the bridge was estimated to be 5%.

4.2 Selection of ground motions

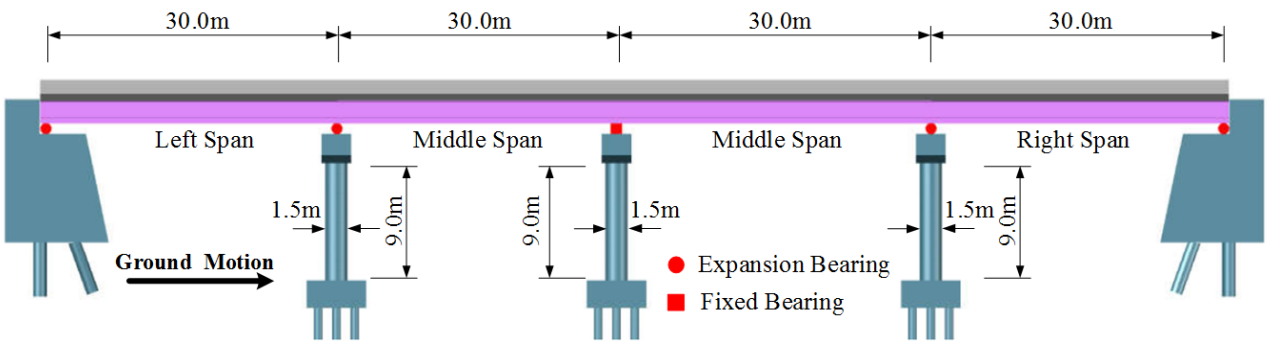

Fig. 7 Elevation of the prototype bridge

In this study, three far-field earthquake records selected from the PEER-NGA Ground Motion Database according to the site classification II [24] were used for the seismic analysis. Table 2 lists the characteristics of the selected ground motions. It should be mentioned that the PGA of three ground motions were scaled to 0.8 g and their durations were extended with an extra duration of 10 s for free vibration to record the residual displacement.

Table 2 – Information of selected ground motions

Site Class	Number	Earthquake	Station	Mw	R_{rup} (km)
II	GM 1	Irpinia, Italy-01	Auletta	6.9	33.10
	GM 2	Loma Prieta	Fremont-Mission	6.4	54.54
	GM 3	Chi-Chi, Taiwai-06	TCU075	6.3	36.04

4.3 Results and discussion

To save space, only the comparison of top displacement of the fixed pier between bridge with initial PT force and without initial PT force subjected to the ground motion 2 is shown in Fig. 8. Fixed piers of both cases reached the maximum displacement around 26.0 s and the residual displacement was at 50.0 s. The maximum displacement and residual displacement of the case without initial PT force were 0.346 m and 0.0174 m, respectively. Compared to the case without initial PT force, the maximum displacement of case with initial PT force increased by 5.7%; however, the residual displacement decreased by 52.3%. This indicated that although the employment of PT force increased the maximum displacement of pier, the recentering capacity enhanced. The amplified maximum displacement response was caused by the decrease of natural period of bridge. The similar phenomenon and trend can also be found in cases of GMs 1 and 3.

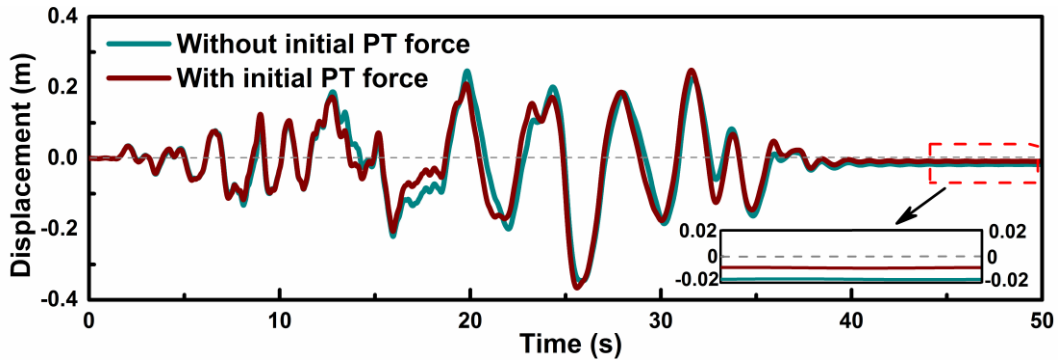

Fig. 8 Displacement response at top of the pier with fixed bearings under GM2.

Fig. 9 compares the later force versus displacement hystereses at the top of the pier with fixed bearings of all selected ground motions. It can be found that the CFST column with initial PT force experienced the

larger lateral displacement and force than those of CFST column without initial PT force. As an example, the maximum displacement and force of fixed pier with initial PT force under GM1 were 0.217 m and 837.21 kN, respectively, which were, respectively, 11.3% and 25.2% larger than those of column without initial PT force. However, the initial PT force can improve the recentering capacity, which was indicated by minor displacement values of the abscissa axis, i.e., the lateral force of 0 kN.

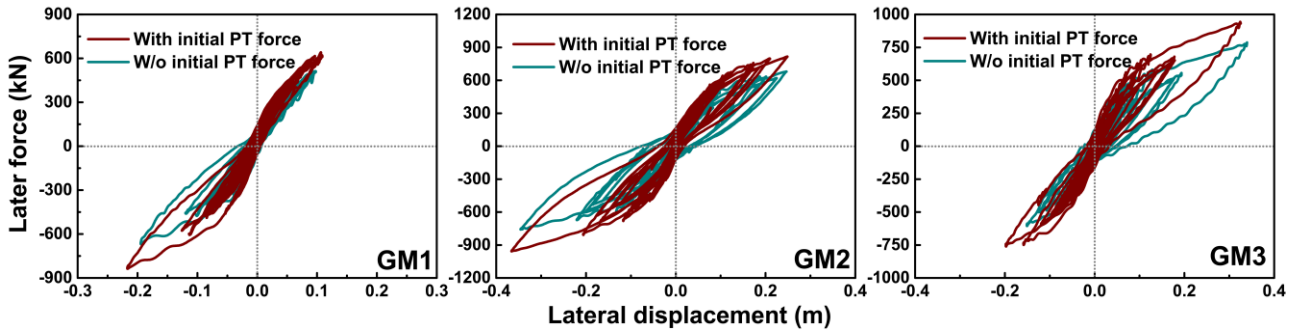

Fig. 9 Lateral force-displacement hystereses of the piers with fixed bearings under selected GMs

5. Summary and Conclusions

This paper presents a numerical analysis for cyclic behavior of posttensioned CFST columns and dynamic response of a typical continuous beam bridge with posttensioned CFST piers. Based on the simulation results, it can be concluded that the load capacity of posttensioned CFST columns was significantly increased by adopting a smaller slenderness ratio and a more amount of ED bars. The energy-dissipated capacity of columns can also be enhanced with abundant ED bars; however, it will result in a larger residual drift and make the columns unacceptable. Consequently, there is a trade-off between the self-centering capacity and energy-dissipation capacity of the hybrid rocking columns. In addition, the use of steel tube for confining the concrete can alleviate the stiffness degradation.

The comparison between time-history analysis results of CFST columns with and without initial PT force demonstrated the benefits of applying initial posttensioning force into the tendon because of the smaller residual drift. However, it should be mentioned that the dynamic response may be amplified, which may result in the pounding between adjacent segment and the unseating failure more easily.

6. Acknowledgements

The authors appreciate the financial support provided by the National Natural Science Foundation of China (Grant NO.51678434 and NO.51838010).

7. References

[1] Guerrini G, Restrepo JI, Massari M, Vervelidis A (2015): Seismic behavior of posttensioned self-centering precast concrete dual-shell steel columns. *Journal of structural engineering*, **141** (4), 04014115.

[2] Yamashita R, Sanders DH (2009): Seismic performance of precast unbonded prestressed concrete columns. *ACI structural journal*, **106** (6), 821-830.

[3] Kurama YC, Sritharan S, Fleischman RB, Restrepo JI, Henry RS, Cleland NM, Ghosh SK, Bonelli P (2018): Seismic-resistant precast concrete structures: state of the art. *Journal of structural engineering*, **144** (4), 03118001.

[4] Mitoulis SA, Rodriguez Rodriguez JR (2017): Seismic performance of novel resilient hinges for columns and application on irregular bridges. *Journal of Bridge Engineering*, **22** (2), 04016114.

[5] Kwan WP, Billington SL (2003): Unbonded posttensioned concrete bridge piers. I: Monotonic and cyclic analyses. *Journal of Bridge Engineering*, **8** (2), 92-101.

[6] Kwan WP, Billington SL (2003): Unbonded posttensioned concrete bridge piers. II: Seismic analyses. *Journal of Bridge Engineering*, **8** (2), 102-111.

[7] Marriott D, Pampanin S, Palermo A (2011): Biaxial testing of unbonded post-tensioned rocking bridge piers with external replacable dissipaters. *Earthquake Engineering & Structural Dynamics*, **40** (15), 1723-1741.

[8] Marriott D, Pampanin S, Palermo A (2009): Quasi-static and pseudo-dynamic testing of unbonded post-tensioned rocking bridge piers with external replaceable dissipaters. *Earthquake engineering & structural dynamics*, **38** (3), 331-354.

[9] Roh H, Ou YC, Kim J, Kim W (2014): Effect of yielding level and post-yielding stiffness ratio of ED bars on seismic performance of PT rocking bridge piers. *Engineering Structures*, **81**, 454-463.

[10] Wang J, Wang Z, Tang Y, Liu T, Zhang J (2018): Cyclic loading test of self-centering precast segmental unbonded posttensioned UHPFRC bridge columns. *Bulletin of Earthquake Engineering*, **16** (11), 5227-5255.

[11] Chou CC, Chang HJ, Hewes JT (2013): Two-plastic-hinge and two dimensional finite element models for post-tensioned precast concrete segmental bridge columns. *Engineering Structures*, **46**, 205-217.

[12] Li C, Hao H, Bi K (2019): Seismic performance of precast concrete-filled circular tube segmental column under biaxial lateral cyclic loadings. *Bulletin of Earthquake Engineering*, **17** (1), 271-296.

[13] Chou CC, Chen YC (2006): Cyclic tests of post-tensioned precast CFT segmental bridge columns with unbonded strands. *Earthquake engineering & structural dynamics*, **35** (2), 159-175.

[14] Li C, Hao H, Bi K (2017): Numerical study on the seismic performance of precast segmental concrete columns under cyclic loading. *Engineering Structures*, **148**, 373-386.

[15] Hayashi K, Skalomenos KA, Inamasu H, Luo YB (2018): Self-Centering Rocking Composite Frame Using Double-Skin Concrete-Filled Steel Tube Columns and Energy-Dissipating Fuses in Multiple Locations. *Journal of Structural Engineering*, **144** (9), 04018146.

[16] Wang XT, Xie CD, Lin LH, Li J (2019): Seismic behavior of self-centering concrete-filled square steel tubular (CFST) Column Base. *Journal of Constructional Steel Research*, **156**, 75-85.

[17] Hassanli R, Youssf O, Mills JE (2017): Seismic performance of precast posttensioned segmental FRP-confined and unconfined crumb rubber concrete columns. *Journal of Composites for Construction*, **21** (4), 04017006.

[18] Tobolski MJ (2010): Improving the design and performance of concrete bridges in seismic regions. *University of California, San Diego*, Ph.D. Thesis, San Diego, USA.

[19] Guerrini G, Restrepo JI, Massari M, Vervelidis A (2012): Self-centering precast concrete dual-shell steel columns. *Proceedings of the 15th World Conference on Earthquake Engineering*, Lisboa, Portugal.

[20] Priestley MJN, Seible F, Benzoni G (1994): Seismic performance of circular columns with low longitudinal steel ratios. Report No. SSRP 94/08, Department of structural engineering, University of California, San Diego, USA.

[21] Han L (2016): *Concrete Filled Steel Tublar Structures-Theory and Practice*. CSPM, 3rd edition.

[22] Qiao Q, Zhang W, Mou B, Cao W (2019): Seismic behavior of exposed concrete filled steel tube column bases with embedded reinforcing bars: Experimental investigation. *Thin-Walled Structures*, **136**, 367-381.

[23] Mander JB, Priestley MJN, Park R (1988): Theoretical stress-strain model for confined concrete. *Journal of structural engineering*, **114** (8), 1804-1826.

[24] MOHURD (2011): *Code for seismic design of urban bridges (CJJ 166–2011)*. China Architecture and Building Press, Beijing.

